PHOTONICS Research

# Synchronization of an optical frequency comb and a microwave oscillator with 53 zs/Hz$^{1/2}$ resolution and 10$^{-20}$-level stability

Changmin Ahn, Yongjin Na, Minji Hyun, Jinho Bae, and Jungwon Kim*

*School of Mechanical and Aerospace Engineering, Korea Advanced Institute of Science and Technology (KAIST), Daejeon 34141, Republic of Korea*
**Corresponding author: jungwon.kim@kaist.ac.kr*

*Received 21 September 2021; revised 16 November 2021; accepted 26 November 2021; posted 30 November 2021 (Doc. ID 443316); published 14 January 2022*

**Precise and stable synchronization between an optical frequency comb (femtosecond mode-locked laser oscillator or microresonator-based comb) and a microwave oscillator is important for various fields including telecommunication, radio astronomy, metrology, and ultrafast X-ray and electron science. Timing detection and synchronization using electro-optic sampling with an interferometer has been actively used for low-noise microwave generation, long-distance timing transfer, comb stabilization, time-of-flight sensing, and laser-microwave synchronization for ultrafast science facilities. Despite its outstanding performance, there has been a discrepancy in synchronization performance of more than 10 dB between the projected shot-noise-limited noise floor and the measured residual noise floor. In this work, we demonstrate the shot-noise-limited performance of an electro-optic timing detector-based comb-microwave synchronization, which enabled an unprecedented residual phase noise floor of −174.5 dBc/Hz at 8 GHz carrier frequency (i.e., 53 zs/Hz$^{1/2}$ timing noise floor), integrated rms timing jitter of 88 as (1 Hz to 1 MHz), rms timing drift of 319 as over 12 h, and frequency instability of $3.6 \times 10^{-20}$ over 10,000 s averaging time. We identified that bandpass filtering of the microwave signal and optical pulse repetition-rate multiplication are critical for achieving this performance.** 

https://doi.org/10.1364/PRJ.443316

## 1. INTRODUCTION

An optical frequency comb, which consists of evenly spaced frequency components in the optical domain, connects the optical and microwave frequencies in a coherent way [1,2]. This unique property has facilitated its utilization to various microwave photonic applications. Precise and stable synchronization between an optical frequency comb (in forms of femtosecond mode-locked lasers or microresonator-based Kerr combs) and a microwave source is important for various fields. It is highly desirable for coherent microwave networks over kilometer (km) distances for very-long-baseline interferometers (VLBIs) [3,4], high-performance optoelectronic phase-locked loops (PLLs) for telecommunications [5], and as a direct link between microwave clocks and optical frequency combs [6]. In particular, it plays a critical role for ultrafast science facilities, such as X-ray free-electron lasers (XFELs) [7,8] and ultrafast electron diffraction (UED) sources [9,10], where precise and stable synchronization between multiple femtosecond mode-locked lasers and microwave-driven cavities and photoguns is required.

Traditionally, the timing error between an optical frequency comb and a microwave source was measured using a microwave mixer after extracting a microwave from the optical pulse train with a high-bandwidth photodetector and a bandpass filter [11–15]. While this method has been widely used, it has limited timing resolution and stability because of the saturation and amplitude-to-phase conversion of photodiodes and the limited phase discrimination resolution of microwave mixers. As an alternative, timing detection in the optical domain using electro-optic sampling with an interferometer has been studied for precise timing discrimination and optical-microwave synchronization [16–22]. There are two optical-microwave timing detection concepts: direct conversion of the timing error into intensity imbalance [16–18,22] and synchronous detection using half of the repetition rate as the modulation signal [19–21]. The former method, which is also collectively called as the electro-optic sampling-based timing detection (EOS-TD) method, has demonstrated subfemtosecond optical-microwave timing synchronization performance [17,22] and high amplitude-to-phase suppression ratio [23] by introducing balanced detection. This approach has been actively used for a variety of applications such as low-noise microwave generation [24,25], long-distance timing transfer [26,27], comb stabilization [6,28], time-of-flight sensing [29], laser-microwave synchronization for UED [30],

and fiber link stabilization for FELs [31]. Despite its excellent performance, there was more than 10 dB difference in synchronization performance between the expected shot-noise-limited noise floor and the measured residual noise floor, indicating that there is still potential for improvement.

In this paper, we demonstrate a shot-noise-limited synchronization performance of the EOS-TD method, which resulted in a single-sideband (SSB) residual phase noise floor of −174.5 dBc/Hz at 8 GHz carrier frequency (i.e., 53 zs/Hz$^{1/2}$ timing noise floor), integrated root-mean-square (rms) timing jitter of 88 as (1 Hz–1 MHz), rms timing drift of 319 as over 12 h, and frequency instability of $3.6 \times 10^{-20}$ over 10,000 s averaging time. We identified that bandpass filtering of the microwave signal and optical pulse repetition-rate multiplication are critical for achieving this performance. To our knowledge, this is the first time to show the combined performance of short-term $< -170$ dBc/Hz-level phase noise and long-term $10^{-20}$-level instability for direct synchronization between an optical frequency comb and a microwave oscillator.

## 2. ELECTRO-OPTIC SAMPLING-BASED TIMING DETECTORS

In this section, we will briefly overview the schematic and operation principles of the EOS-TDs. In essence, the EOS-TD converts the timing error between zero-crossings of the microwave signal and ultrashort optical pulses ($\tau$ in Fig. 1) into the intensity imbalance between the two outputs of the interferometer so that the timing error can be precisely detected by a balanced photodetector (BPD) (see Fig. 1). The standard configuration of the EOS-TD is based on an asymmetric-phase-biased fiber interferometer, which consists of a $2 \times 2$ optical coupler with 50:50 coupling ratio, a traveling-wave electro-optic phase modulator (EOM), and a unidirectional $\pi/2$ phase bias [Fig. 1(a)] [17]. When the optical phase difference between the two counterpropagating pulses is $\Delta\phi$, the two outputs from the Sagnac loop are proportional to $\cos^2(\Delta\phi/2)$ and $\sin^2(\Delta\phi/2)$. In order to bias the Sagnac loop in the balanced condition, a nonreciprocal $\pi/2$ phase bias unit is inserted in the loop. The resulting optical phase difference is $\Delta\phi = \phi_E + \pi/2$, where $\phi_E$ is the optical phase induced by the EOM, which is proportional to the timing error ($\tau$) between the microwave and the optical pulses. Here, as the traveling-wave EOM is used, the unidirectionality is guaranteed for gigahertz (GHz) microwave signals. The two Sagnac-loop outputs are detected by the BPD to obtain the timing error with minimal impact of intensity noise. Note that, in the actual implementation, an attenuator is required to compensate for the power imbalance caused by the circulator. To convert the BPD output voltage ($V_{\text{out}}$) into timing error, the timing detection sensitivity [$K_d$ in volts per second (V/s)] of the EOS-TD should be measured. The detection sensitivity can be determined from the zero-crossing slope of the BPD output voltage when the PLL is not activated, which is an error signal with frequency of $|Nf_{\text{rep}} - f_{\text{VCO}}|$. The lower the half-wave voltage ($V_\pi$) of the EOM, the higher the microwave power applied to the EOM, and the higher the input optical power increases the detection sensitivity $K_d$. When the output from the BPD is applied to a microwave voltage-controlled oscillator (VCO) via a loop filter [such as a proportional-integral (PI) servo controller], one can synchronize a microwave VCO to an optical frequency comb. Inversely, synchronization of an optical frequency comb to a master microwave oscillator is also possible by applying the BPD output to the repetition-rate tuning actuator [such as a piezoelectric transducer-mounted mirror] in the comb source.

The same EOS-TD principle can be implemented with different configurations. For example, a $3 \times 3$ optical coupler-based

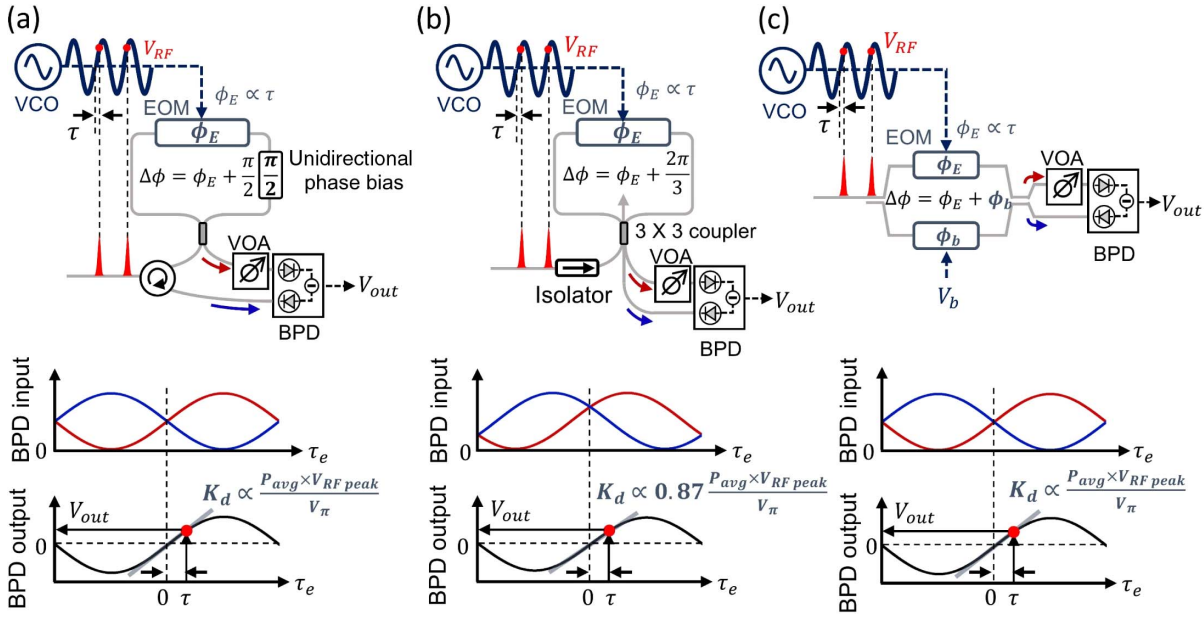


**Fig. 1.** Schematic of EOS-TDs. (a) Sagnac-loop-based EOS-TD with unidirectional phase bias, (b) $3 \times 3$ optical coupler-based EOS-TD, (c) DO-MZM-based EOS-TD. VCO, voltage-controlled oscillator; BPD, balanced photodetector; EOM, electro-optic phase modulator; VOA, variable optical attenuator.

EOS-TD [22] [Fig. 1(b)] was demonstrated. Here, the 3 × 3 optical coupler provides a $2\pi/3$ phase shift between ports, which enables the self-biasing of the interferometer at the expense of slightly degraded detection sensitivity. By eliminating the magneto-optic component-based $\pi/2$ bias unit in the Sagnac loop, this configuration has the potential for realizing the EOS-TD in an integrated photonic platform. Another EOS-TD implementation method is using a dual-output Mach–Zehnder modulator (DO-MZM) [18,25] [Fig. 1(c)], where the phase bias ($\phi_b$) is provided by the bias voltage ($V_b$) applied to the modulator. While its long-term stability is compromised by the stability of the bias voltage, it can still provide a high detection sensitivity and good short-term performance. As different configurations have their own cons and pros, one can select the proper EOS-TD method depending on the intended applications. Note that, in this paper, we used the standard 2 × 2 coupler-based EOS-TDs for synchronization experiments.

## 3. EXPERIMENT METHODS

Figure 2 shows an overall setup of the EOS-TD-based timing synchronization experiment. A 250 MHz mode-locked erbium-doped fiber laser oscillator (FC1500-250-ULN, MenloSystems GmbH) was used for the optical pulse source. The optical signal goes through dispersion compensating fibers (DCFs), which adjust the pulse duration incident at the EOM below 1 ps for accurate electro-optic sampling. We multiplied the pulse repetition rate using a multistage ($m = 1, 2, 3$) Mach–Zehnder interferometer (MZI) to study the repetition-rate dependence [32]. Note that 1-stage, 2-stage, and 3-stage MZI corresponds to pulse repetition rates of 500 MHz, 1 GHz, and 2 GHz, respectively. The optical signal was amplified by a homemade erbium-doped fiber amplifier (EDFA) to ~60 mW. To suppress the impact of relative intensity noise (RIN), a laser diode current controller-based RIN stabilization scheme was adopted by tapping 5% of optical power at the EDFA output. The amplified optical signal was divided into two parts by a 50:50 optical fiber coupler to synchronize the microwave oscillator to the optical pulse train (in-loop) and, at the same time, evaluate the synchronization performance (out-of-loop). Both EOS-TDs were constructed with low-$V_\pi$ EOMs for sensitive optical-microwave timing error detection. To avoid the saturation of the balanced photodetector at the EOS-TD output, the optical power incident at each BPD port was adjusted to ~4 mW, which is lower than the specified saturation power (4.5 mW) of the used BPD (Thorlabs PDB450C).

For constructing the synchronization PLL, the output voltage of the in-loop EOS-TD is fed to a loop filter (LB-1005, Newfocus), which is a PI controller. The controller output is applied to an 8 GHz VCO (HMC-C200, Hittite), which is used as a slave microwave oscillator. Here, the VCO frequency should be matched to the multiples of pulse repetition rate ($N f_{rep}$). The microwave signal from the VCO was amplified by a radio-frequency (RF) amplifier (NBL00437, Nextec-RF) to maximize the detection sensitivity of the EOS-TD. We suppressed other harmonic frequency components of the VCO using an RF bandpass filter (6C52-8000/T200-O/O, K&L Microwave). This microwave signal was split and distributed to each EOM of the in-loop and out-of-loop EOS-TDs. Here, to reduce the environmental effect, such as air fluctuation and temperature change caused by an air conditioner, the experimental setup was placed inside a polycarbonate shielding box.

The residual phase noise of the synchronization PLL was evaluated by the out-of-loop EOS-TD. The voltage noise power spectra were measured by a fast Fourier transform (FFT) spectrum analyzer (SR760, Stanford Research Systems) and an RF spectrum analyzer (E4440A, Keysight) for the offset frequency range of 1 Hz–100 kHz and 100 kHz–10 MHz, respectively, and converted to the equivalent timing and phase noise power spectral densities (PSDs). The measurement was performed at the zero-crossing of the out-of-loop EOS-TD output

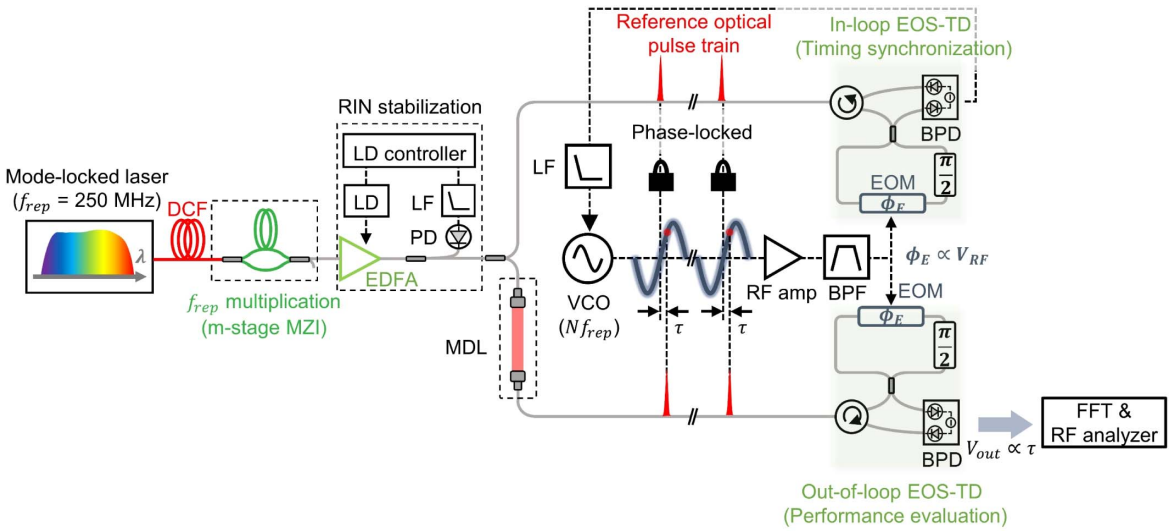


**Fig. 2.** Experimental setup schematic of the optical–microwave timing synchronization. DCF, dispersion compensating fiber; MZI, Mach–Zehnder interferometer; LF, loop filter; MDL, manual delay line; BPD, balanced photodetector; PD, photodetector; EDFA, erbium-doped fiber amplifier; RIN, relative intensity noise; LD, laser diode; VCO, voltage-controlled oscillator; BPF, bandpass filter; EOM, electro-optic phase modulator; RF amp, RF amplifier.

by controlling the relative optical path difference with a manual delay line (MDL in Fig. 2) to maximize the detection sensitivity and suppress the impact of intensity noise.

## 4. MEASUREMENT RESULTS

### A. Effect of Bandpass Filtering of the Microwave Signal

In this work, we first checked the effect of RF bandpass filtering. Ideally, the microwave oscillator should generate a single-tone microwave (8 GHz in this work); however, as shown in Fig. 3(a), harmonic modes of 8 GHz, such as 16 GHz and 24 GHz, are also generated due to the nonlinearity of the oscillator. As the RF spectrum of the frequency comb contains the harmonics of its repetition rate, harmonic modes of the microwave oscillator ($2f_{\mathrm{VCO}}$) might be downconverted by its nearest RF mode of mode-locked laser ($2Nf_{\mathrm{rep}}$) and deteriorate the timing error signal. To minimize this effect, an 8 GHz bandpass filter (BPF) with 200 MHz bandwidth is inserted after the RF amplifier (see Fig. 2).

We compared the phase noise with and without the RF-BPF for both 250 MHz and 2 GHz pulse repetition-rate cases [Fig. 3(b)]. When the repetition rate is 250 MHz, the phase noise PSDs at 100 kHz offset frequency without [curve (i)] and with [curve (ii)] RF-BPF were measured to be −153 dBc/Hz (629 zs/Hz$^{1/2}$) and −169 dBc/Hz (100 zs/Hz$^{1/2}$), respectively. When the repetition rate is increased to 2 GHz, the corresponding residual phase noise without and with RF-BPF was −165 dBc/Hz [158 zs/Hz$^{1/2}$, curve (iii)] and −174.5 dBc/Hz [53 zs/Hz$^{1/2}$, curve (iv)], respectively. For both repetition-rate cases, the phase noise is reduced by more than 10 dB when the RF-BPF is used. This improved phase noise level corresponds to the calculated shot-noise limit of the in-loop EOS-TD [dashed lines in Fig. 3(b)], which is $S_{\mathrm{shot}} = \frac{2qiG^2}{K_d^2}$ (rad$^2$/Hz), where $q$ is the charge of electron (C), $i$ is the average current at each photodiode in the BPD (A), $G$ is the transimpedance gain of the BPD (V/A), and $K_d$ is the measured detection sensitivity (V/rad or V/s). Note that, in this experiment, because a higher-$V_\pi$ EOM is used for in-loop EOS-TD (therefore having lower $K_d$), the in-loop EOS-TD determines the shot-noise-limited noise floor. From this experiment, we found that making a single-tone microwave signal is critical for achieving the shot-noise-limited performance of the EOS-TD-based synchronization.

### B. Optical Pulse Repetition-Rate Dependence

The repetition-rate dependence of the EOS-TD is also studied. For this, we conducted the same experiment with different repetition rates of 250 MHz, 500 MHz, 1 GHz, and 2 GHz by changing the number of MZI pulse interleaving stages in Fig. 2. For each case, the pulse duration at the EOS-TD input is adjusted to be <1 ps using different lengths of DCFs. The RF-BPF (described in Section 4.A) is used for all cases.

Figure 4(a) shows the measured detection sensitivity ($K_d$) when the pulse repetition rate is increased from 250 MHz to 2 GHz with the same average optical power incident at the BPD (4 mW to each photodiode). The measured detection sensitivity of out-of-loop EOS-TD is 14 V/rad (0.7 mV/fs), 17 V/rad (0.85 mV/fs), 24 V/rad (1.2 mV/fs), and 30 V/rad (1.5 mV/fs) for 250 MHz, 500 MHz, 1 GHz, and 2 GHz repetition rates, respectively. The repetition-rate dependence of detection sensitivity is due to the increase of effective RF mode power at 8 GHz of optical pulse train. The error signal from the BPD output, an aliased VCO signal, can be treated as the downconversion of microwave signal by the interaction with the nearest RF mode of the optical pulse train. Therefore, to enhance the SNR of this error signal, increasing the nearest mode power of optical pulse train at $f_{\mathrm{VCO}}$ is required. As the RF mode power increases for higher-repetition-rate pulses, the detection sensitivity increases. We believe that the detection sensitivity will be saturated at some point as the BPD is saturated above a certain mode power threshold.

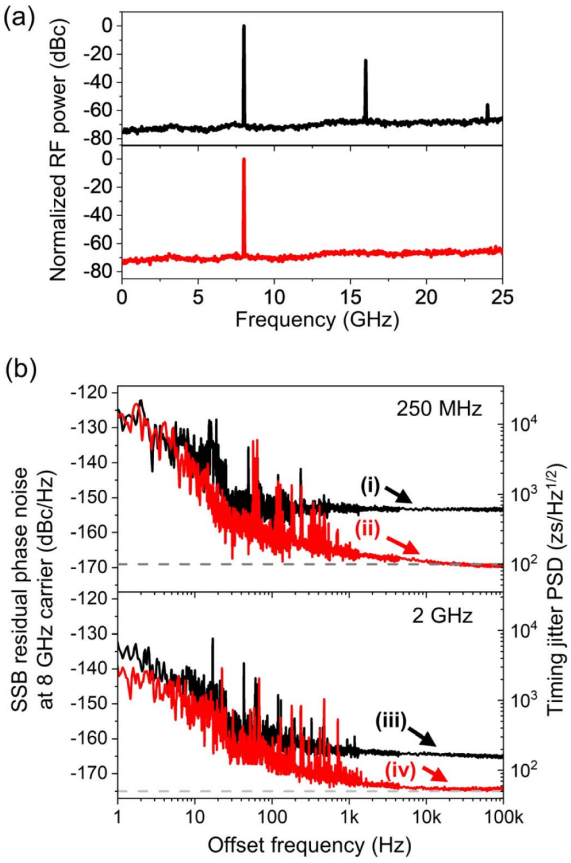


**Fig. 3.** (a) RF spectrum of the 8 GHz VCO output without (black) and with RF bandpass filtering (red). (b) SSB residual phase noise at 8 GHz carrier [curve (i), curve (iii)] without and [curve (ii), curve (iv)] with the RF bandpass filter when repetition rate is 250 MHz and 2 GHz, respectively. Here, the dashed line is the shot limit of the in-loop EOS-TD.

Figure 4(b) shows the measured SSB phase noise floors for different repetition-rate conditions, where curves (i), (ii), (iii), and (iv) correspond to the residual phase noise floor with pulse repetition rate of 250 MHz, 500 MHz, 1 GHz, and 2 GHz, respectively. The residual phase noise at 100 kHz offset frequency decreases from −168 dBc/Hz (112 zs/Hz$^{1/2}$) to −170 dBc/Hz (89 zs/Hz$^{1/2}$), −172.5 dBc/Hz (67 zs/Hz$^{1/2}$), and −174.5 dBc/Hz (53 zs/Hz$^{1/2}$) when the repetition rate increases from 250 to 500 MHz, 1 GHz, and 2 GHz. These

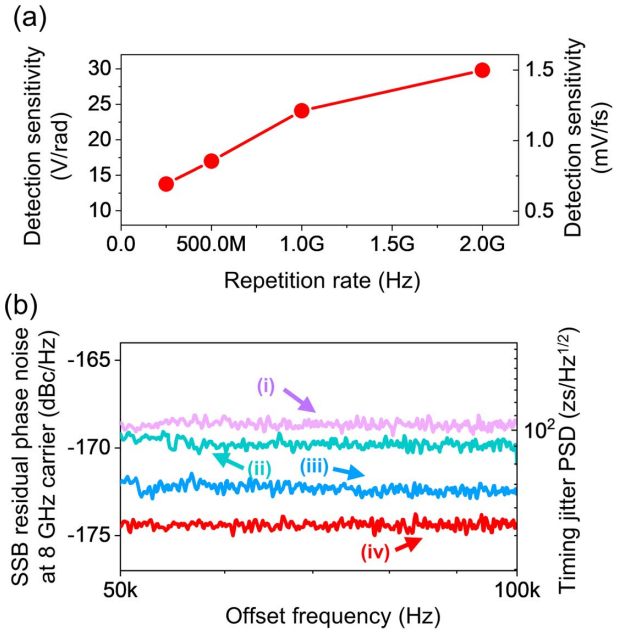


**Fig. 4.** (a) Change of detection sensitivity for different pulse repetition rates. (b) SSB phase noise floor at 8 GHz carrier [curve (i)] without MZI, [curve (ii)] with 1-stage, [curve (iii)] 2-stage, and [curve (iv)] 3-stage MZI, respectively.

measured noise levels agree fairly well with the computed shot-noise-limited levels [$S_{shot}(f)$].

Figure 5 shows the measured SSB residual phase noise and integrated rms timing jitter of the EOS-TD-based timing synchronization when both the RF-BPF and three-stage MZI are employed. Curves (i) and (ii) show the free-running VCO phase noise and the residual phase noise for comb-microwave synchronization, respectively. The residual phase noise at 8 GHz carrier reaches −174.5 dBc/Hz at 100 kHz offset frequency, which corresponds to 53 zs/Hz$^{1/2}$ timing jitter PSD. Owing to this low residual phase noise, the rms integrated timing jitter was 88 as (1 Hz–1 MHz) [2.68 fs (1 Hz–10 MHz)]. The phase noise floor is mostly limited by shot noise from the BPD detecting the in-loop EOS-TD output (dashed line in Fig. 5). In the frequency range below 1 kHz, the measurement limit of out-of-loop EOS-TD dominates. At the high offset frequency above 1 MHz, there is a strong resonant peak caused by the limited phase margin and free-running VCO phase noise that is much higher than the EOS-TD noise floor.

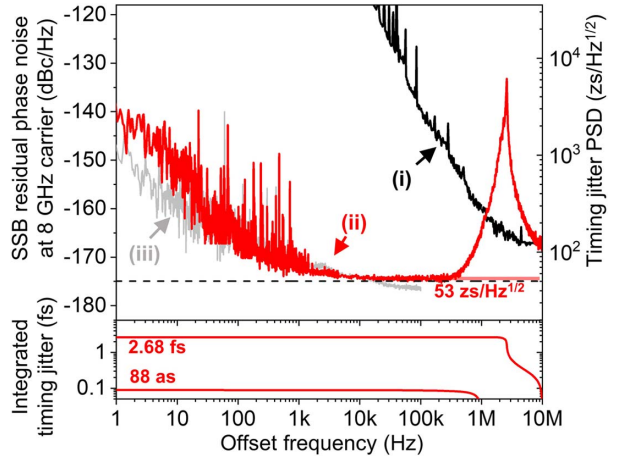


**Fig. 5.** SSB phase noise at 8 GHz carrier and integrated timing jitter with the experimental setup of Fig. 1. Curve (i) denotes the phase noise of free-running VCO, curve (ii) denotes the phase noise after timing synchronization, and curve (iii) denotes the measurement background of the out-of-loop EOS-TD. The dashed line is a calculated shot-noise limit of the in-loop EOS-TD. The red line at the bottom graph indicates the integrated timing jitter of curve (ii).

### C. Impact of the Lead Compensator

As mentioned in the previous section, the high resonance peak caused by the control loop makes large integrated timing jitter for a higher integration frequency range. Therefore, we designed an additional lead compensator to increase the phase margin at a few megahertz (MHz), which leads to a lower resonance peak. The lead compensator was designed using passive components, including a resistor and a capacitor, and placed before the loop filter. For the experiment, the RF-BPF and three-stage MZI were used.

The measurement results are shown in Fig. 6. Curves (i) and (ii) indicate the SSB residual phase noise with and without the lead compensator, respectively. For comparison, the phase noise of the free-running VCO is also shown [curve (iii)]. As there is no change in the in-loop measurement noise floor, two data have the same phase noise of −174.5 dBc/Hz (53 zs/Hz$^{1/2}$) at 10 kHz offset frequency. However, by the effect of the lead compensator, the resonance peak is reduced to −155 dBc/Hz (500 zs/Hz$^{1/2}$), which is improved by ∼20 dB compared to the case without the lead compensator. We also compared the corresponding integrated timing jitter for each case, which is shown in the bottom figure. When the lead compensator was applied, the integrated timing jitter was 716 as over 10 MHz integrated bandwidth, which was improved by a factor of 3.7. The resonance peak level and the control bandwidth can be also improved by using a microwave oscillator with lower free-running phase noise and/or higher frequency modulation bandwidth.

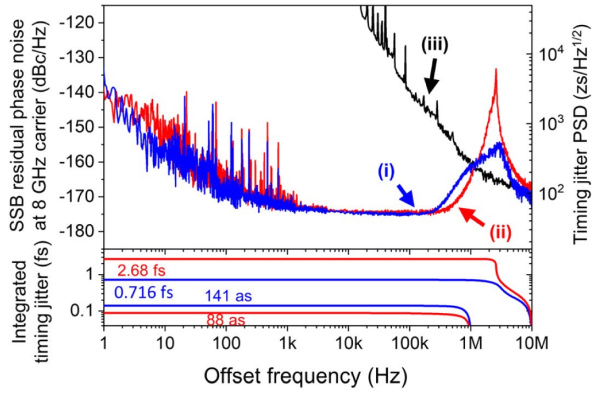


**Fig. 6.** SSB residual phase noise at 8 GHz carrier and integrated timing jitter. Curve (i), curve (ii) indicate the residual phase noise with and without the lead compensator, respectively. The phase noise of the VCO is also shown [curve (iii)]. Integrated timing jitters of curves (i), (ii) correspond to blue and red curves, respectively.

### D. Long-Term Stability Evalution

The long-term stability of the EOS-TD-based optical-microwave timing synchronization system was evaluated (Fig. 7). Note that this experiment was conducted with the RF BPF and the three-stage MZI. The relative timing error was acquired by monitoring the out-of-loop EOS-TD output using a data acquisition board with 100 Hz sampling rate. Note that we placed the experimental setup (except the comb source) inside a polycarbonate shielding box to isolate the external effects such as temperature change and air fluctuations. For the long-term measurement, we turned on the entire setup and waited for ~1 day to reach the steady state at temperature inside the shielding box. The resulting temperature stability is shown in Fig. 7(a), where the temperature varied over ~0.06–0.2 K peak to peak (0.015–0.059 K rms) over 12 h.

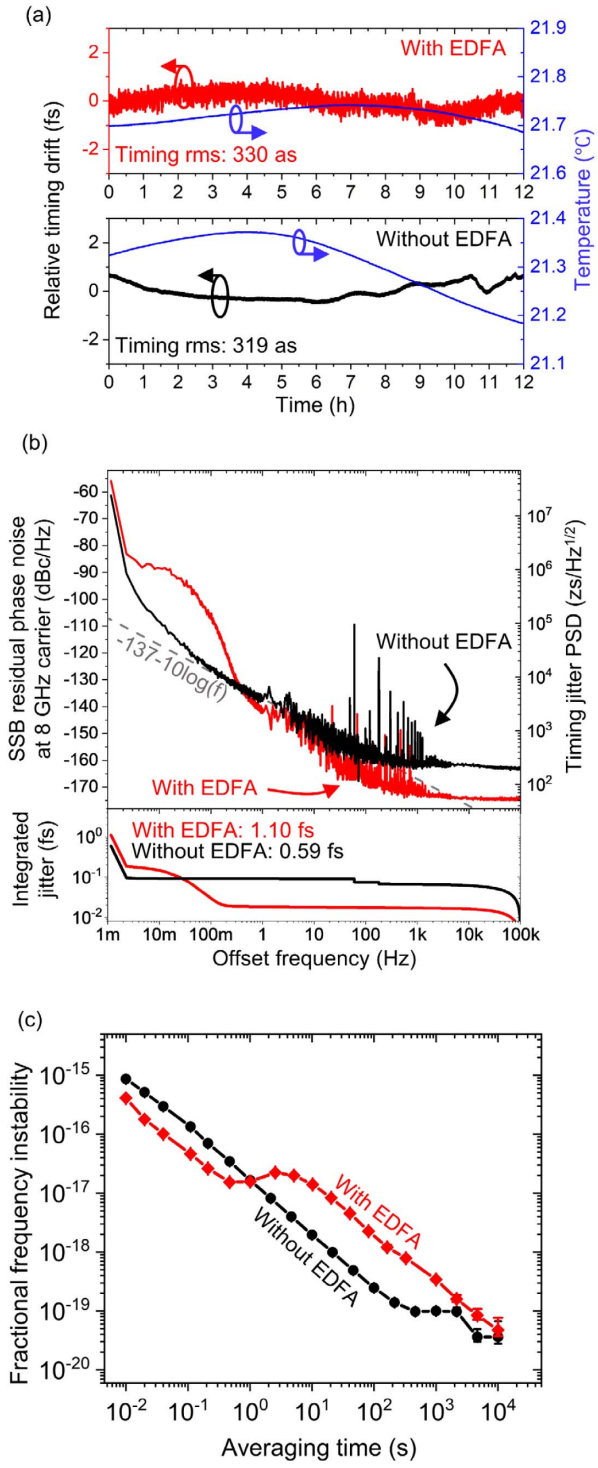


**Fig. 7.** Long-term stability evaluation results. (a) Relative timing error measured for 12 h, (b) residual phase noise and integrated jitter down to 1 mHz offset frequency, and (c) fractional frequency instability (overlapping Allan deviation).

We first used the same test condition as that for obtaining the short-term measurement results (Figs. 3–6). As can be seen in Fig. 7(c), there is an instability bump around 0.2–20 s averaging time (the "with EDFA" case). Note that similar bump in this time scale was also observed and reported by other previous research, and it was attributed to technical noise induced by feedback control [33,34]. In this work, we carefully examined the possible causes of the frequency instability bump in our synchronization system and found that gain condition of the EDFA pump's thermoelectric cooler (TEC) control was the primary cause. Thus, we also evaluated the long-term synchronization performances without the EDFA. Comparisons of the timing drift over 12 h, the equivalent phase noise PSD down to 1 mHz offset frequency, and the frequency instability over 10,000 s averaging time are shown in Figs. 7(a), 7(b), and 7(c), respectively.

First, as shown in Fig. 7(a), removing the EDFA greatly reduces the thickness of the timing drift data, owing to significantly reduced noise in the 0.2–20 s time scale. The integrated rms timing drift over 12 h is 319 as (without EDFA) and 330 as (with EDFA). The temperature of the EOS-TD was also monitored and maintained within 0.06–0.2 K over 12 h. As the measured timing drift shows a certain degree of correlation with the temperature (with ~–0.75 corrrelation coefficient for the "without EDFA" case), we believe that the major limiting factor for the long-term drift over several hours is the temperature drift of the synchronization system.

Figure 7(b) shows the residual phase noise and integrated jitter extended down to 1 mHz offset frequency. When the EDFA is used, a bump in phase noise in the 2 mHz–1 Hz range is clearly visible, which corresponds to the thick timing drift data [in Fig. 7(a)] and bump in frequency instability [in Fig. 7(c)]. By removing the EDFA, the bump in the 2 mHz–1 Hz frequency range is removed, and the phase noise follows a slope of −10 dB/decade down to <200 mHz. This corresponds to the flicker noise of −137 dBc/Hz at 1 Hz, which might be originated from the BPD in the EOS-TD. Note that, when the EDFA is not used, due to the limited input optical power to the EOS-TD, the high-frequency white phase noise floor becomes worse from −174.5 to −163 dBc/Hz. Thus, there is a trade-off between the high-frequency noise floor and the low-frequency noise bump when using the EDFA in the synchronization setup.

In Fig. 7(c), the relative timing error was also converted into fractional frequency instability in terms of overlapping Allan deviation. Fractional frequency instability reached $4.7 \times 10^{-20}$ ($3.6 \times 10^{-20}$) over 10,000 s averaging time with EDFA (without EDFA). As discussed earlier, a bump in the

0.2–20 s averaging time could be removed by eliminating the EDFA and follows the inverse of averaging time up to ∼200 s. Compared with one of the state-of-the-art optical-to-microwave links [35], this method shows comparable (with EDFA) or ∼8 times better (without EDFA) fractional frequency instability at 100 s. Overall, the use of EDFA increases the optical power and leads to better short-term performance. On the other hand, the instabtiliy caused by the pump diode controller for the EDFA generates additional noise in the 0.2–20 s time scale, and therefore removing the EDFA can enhance the long-term frequency stability. More stable temperature environment around the pump laser diode and better active temperature control may further improve the frequency stability.

## 5. CONCLUSION

In summary, we have demonstrated the shot-noise-limited performance of the EOS-TD-based synchronization between an optical frequency comb and a microwave oscillator, which enabled unprecedented residual phase noise floor of −174.5 dBc/Hz at 8 GHz carrier frequency (i.e., 53 zs/$Hz^{1/2}$ timing noise floor), integrated rms timing jitter of 88 as (1 Hz–1 MHz), minimum rms timing drift of 319 as over 12 h, and frequency instability of $3.6 \times 10^{-20}$ over 10,000 s averaging time. We identified that bandpass filtering of the microwave signal and optical pulse repetition-rate multiplication are critical for achieving this performance. The demonstrated method shows excellent comb-microwave synchronization performance for both short-term resolution and long-term stability, which will be useful for various fields such as ultrafast X-ray and electron science instrumentation, radio astronomy, telecommunications, and precision metrology.

**Funding.** National Research Foundation of Korea (NRF-2021R1A2B5B03001407, NRF-2021R1A5A1032937).

**Disclosures.** The authors declare no conflicts of interest.

**Data Availability.** Data underlying the results presented in this paper are not publicly available at this time but may be obtained or accessed in the future.

## REFERENCES

1. T. Udem, R. Holzwarth, and T. W. Hänsch, "Optical frequency metrology," Nature **416**, 233–237 (2002).
2. A. D. Ludlow, M. M. Boyd, J. Ye, E. Peik, and P. O. Schmidt, "Optical atomic clocks," Rev. Mod. Phys. **87**, 637–701 (2015).
3. C. Clivati, R. Aiello, and G. Bianco *et al.*, "Common-clock very long baseline interferometry using a coherent optical fiber link," Optica **7**, 1031–1037 (2020).
4. C. Clivati, R. Ambrosini, T. Artz, A. Bertarini, C. Bortolotti, M. Frittelli, F. Levi, A. Mura, G. Maccaferri, M. Nanni, M. Negusini, F. Perini, M. Roma, M. Stagni, M. Zucco, and D. Calonico, "A VLBI experiment using a remote atomic clock via a coherent fibre link," Sci. Rep. **7**, 40992 (2017).
5. J. C. Scheytt, D. Wrana, M. Bahmanian, and I. Kallfass, "Ultra-low phase noise frequency synthesis for THz communications using optoelectronic PLLs," in *3rd International Workshop on Mobile Terahertz Systems (IWMTS)* (2020), pp. 1–4
6. S. Zhang, J. Wu, J. Leng, S. Lai, and J. Zhao, "Highly precise stabilization of intracavity prism-based Er:fiber frequency comb using optical-microwave phase detector," Opt. Lett. **39**, 6454–6457 (2014).
7. P. Emma, R. Akre, J. Arthur, and R. Bionta, "First lasing and operation of an ångstrom-wavelength free-electron laser," Nat. Photonics **4**, 641–647 (2010).
8. S. Schulz, I. Grguraš, C. Behrens, H. Bromberger, J. T. Costello, M. K. Czwalinna, M. Felber, M. C. Hoffmann, M. Ilchen, H. Y. Liu, T. Mazza, M. Meyer, S. Pfeiffer, P. Predki, S. Schefer, C. Schmidt, U. Wegner, H. Schlarb, and A. L. Cavalieri, "Femtosecond all-optical synchronization of an X-ray free-electron laser," Nat. Commun. **6**, 5938 (2015).
9. J. Shin, H. Kim, S. Park, H. Bark, K. Oang, K. Jang, K. Lee, F. Rotermund, Y. Jeong, and J. Kim, "Sub-10-fs timing for ultrafast electron diffraction with THz-driven streak camera," Laser Photon. Rev. **15**, 2000326 (2021).
10. S. P. Weathersby, G. Brown, M. Centurion, T. F. Chase, R. Coffee, J. Corbett, J. P. Eichner, J. C. Frisch, A. R. Fry, M. Gühr, N. Hartmann, C. Hast, R. Hettel, R. K. Jobe, E. N. Jongewaard, J. R. Lewandowski, R. K. Li, A. M. Lindenberg, I. Makasyuk, J. E. May, D. McCormick, M. N. Nguyen, A. H. Reid, X. Shen, K. Sokolowski-Tinten, T. Vecchione, S. L. Vetter, J. Wu, J. Yang, H. A. Dürr, and X. J. Wang, "Mega-electron-volt ultrafast electron diffraction at SLAC National Accelerator Laboratory," Rev. Sci. Instrum. **86**, 073702 (2015).
11. R. P. Scott, C. Langrock, and B. H. Kolner, "High-dynamic-range laser amplitude and phase noise measurement techniques," IEEE J. Sel. Top. Quantum Electron. **7**, 641–655 (2001).
12. F. Kiewiet, A. Kemper, O. Luiten, G. Brussaard, and M. J. van der wiel, "Femtosecond synchronization of a 3 GHz RF oscillator to a mode-locked Ti:sapphire laser," Nucl. Instrum. Methods Phys. Res. Sect. A **484**, 619–624 (2002).
13. Q. Du, Y. Du, L. Yan, W. Huang, J. Li, and C. Tang, "Precise control and measurement of Laser-RF synchronization for Thomson-scattering X-ray source," Nucl. Instrum. Methods Phys. Res. Sect. A **637**, S137–S140 (2011).
14. K. Gumerlock, J. Frisch, B. Hill, J. May, D. Nelson, and S. Smith, "A low-cost, high-reliability femtosecond laser timing system for LCLS," in *36th International Free Electron Laser Conference (FEL)* (2014), pp. 917–921.
15. M. Titberidze, M. Felber, T. Lamb, R. Loch, C. Sydlo, and H. Schlarb, "Fs level laser-to-RF synchronization at REGAE," J. Phys. Conf. Ser. **874**, 012085 (2017).
16. J. Kim, M. H. Perrott, and F. X. Kaertner, "Femtosecond synchronization of RF-signals with optical pulse trains," Opt. Lett. **79**, 768–770 (2004).
17. K. Jung and J. Kim, "Subfemtosecond synchronization of microwave oscillators with mode-locked Er-fiber lasers," Opt. Lett. **37**, 2958–2960 (2012).
18. M. Endo, T. D. Shoji, and T. R. Schibli, "High-sensitivity optical to microwave comparison with dual-output Mach-Zehnder modulators," Sci. Rep. **8**, 4388 (2018).
19. M. Y. Peng, A. Kalaydzhyan, and F. X. Kärtner, "Balanced optical-microwave phase detector for sub-femtosecond optical-RF synchronization," Opt. Express **22**, 21702–21711 (2014).
20. M. Xin, K. Şafak, M. Y. Peng, A. Kalaydzhyan, W. T. Wang, O. D. Mücke, and F. X. Kärtner, "Attosecond precision multi-kilometer laser-microwave network," Light Sci. Appl. **6**, e16187 (2017).
21. A. Nejadmalayeri and F. Kärtner, "Mach-Zehnder based balanced optical microwave phase detector," in *Conference on Lasers and Electro-Optics* (2012), paper CTu2A.1.
22. C.-G. Jeon, Y. Na, B.-W. Lee, and J. Kim, "Simple-structured, subfemtosecond- resolution optical-microwave phase detector," Opt. Lett. **43**, 3997–4000 (2018).
23. M. Lessing, H. S. Margolis, C. T. A. Brown, P. Gill, and G. Marra, "Suppression of amplitude-to-phase noise conversion in balanced optical-microwave phase detectors," Opt. Express **21**, 27057–27062 (2013).
24. D. Hou, X. P. Xie, Y. L. Zhang, J. T. Wu, Z. Y. Chen, and J. Y. Zhao, "Highly stable wideband microwave extraction by synchronizing widely tunable optoelectronic oscillator with optical frequency comb," Sci. Rep. **3**, 3509 (2013).

25. M. Bahmanian and J. C. Scheytt, "A 2–20-GHz ultralow phase noise signal source using a microwave oscillator locked to a mode-locked laser," IEEE Trans. Microw. Theory Tech. **69**, 1635–1645 (2021).
26. X. Chen, J. Zhang, J. Lu, X. Lu, X. Tian, B. Liu, H. Wu, T. Tang, K. Shi, and Z. Zhang, "Feed-forward digital phase compensation for long-distance precise frequency dissemination via fiber network," Opt. Lett. **40**, 371–374 (2015).
27. X. Chen, J. Lu, Y. Cui, J. Zhang, X. Lu, X. Tian, C. Ci, B. Liu, H. Wu, T. Tang, K. Shi, and Z. Zhang, "Simultaneously precise frequency transfer and time synchronization using feed-forward compensation technique via 120 km fiber link," Sci. Rep. **5**, 18343 (2015).
28. B. Ning, S. Zhang, D. Hou, J. Wu, Z. Li, and J. Zhao, "High-precision distribution of highly stable optical pulse trains with $8.8\times10^{-19}$ instability," Sci. Rep. **4**, 5109 (2014).
29. Y. Na, C. G. Jeon, C. Ahn, M. Hyun, D. Kwon, J. Shin, and J. Kim, "Ultrafast, sub-nanometre-precision and multifunctional time-of-flight detection," Nat. Photonics **14**, 355–360 (2020).
30. H. Yang, B. Han, J. Shin, D. Hou, H. Chung, I. Baek, Y. Jeong, and J. Kim, "10-fs-level synchronization of photocathode laser with RF-oscillator for ultrafast electron and X-ray sources," Sci. Rep. **7**, 39966 (2017).
31. K. Jung, J. Lim, J. Shin, H. Yang, L. Chen, F. X. Kaertner, H. Kang, C. Min, and J. Kim, "Remote laser-microwave synchronization over kilometer-scale fiber link with few-femtosecond drift," J. Lightwave Technol. **32**, 3742–3748 (2014).
32. A. Haboucha, W. Zhang, T. Li, M. Lours, A. N. Luiten, Y. Le Coq, and G. Santarelli, "Optical-fiber pulse rate multiplier for ultralow phase-noise signal generation," Opt. Lett. **36**, 3654–3656 (2011).
33. J. Millo, R. Boudot, M. Lours, P. Y. Bourgeois, A. N. Luiten, Y. Le Coq, Y. Kersale, and G. Santarelli, "Ultra-low noise microwave extraction from fiber-based optical frequency comb," Opt. Lett. **34**, 3707–3709 (2009).
34. N. Hinkley, J. A. Sherman, N. B. Phillips, M. Schioppo, N. D. Lemke, K. Beloy, M. Pizzocaro, C. W. Oates, and A. D. Ludlow, "An atomic clock with $10^{-18}$ instability," Science **341**, 1215–1218 (2013).
35. T. Nakamura, J. Davila-Rodriguez, H. Leopardi, J. A. Sherman, T. M. Fortier, X. Xie, J. C. Campbell, W. F. McGrew, X. Zhang, Y. S. Hassan, D. Nicolodi, K. Beloy, A. D. Ludlow, S. A. Diddams, and F. Quinlan, "Coherent optical clock down-conversion for microwave frequencies with $10^{-18}$ instability," Science **368**, 889–892 (2020).